ELSEVIER

Contents lists available at ScienceDirect

# **Mathematical Biosciences**

journal homepage: www.elsevier.com/locate/mbs



# Ca<sup>2+</sup>-activation kinetics modulate successive puff/spark amplitude, duration and inter-event-interval correlations in a Langevin model of stochastic Ca<sup>2+</sup> release



Xiao Wang\*, Yan Hao, Seth H. Weinberg, Gregory D. Smith

Department of Applied Science, The College of William and Mary, Williamsburg, VA 23187, United States

#### ARTICLE INFO

Article history: Received 18 December 2014 Revised 16 March 2015 Accepted 27 March 2015 Available online 2 April 2015

Keywords: Ca<sup>2+</sup> puffs Ca<sup>2+</sup> sparks Langevin equation Markov chain

#### ABSTRACT

Through theoretical analysis of the statistics of stochastic calcium ( $Ca^{2+}$ ) release (i.e., the amplitude, duration and inter-event interval of simulated  $Ca^{2+}$  puffs and sparks), we show that a Langevin description of the collective gating of  $Ca^{2+}$  channels may be a good approximation to the corresponding Markov chain model when the number of  $Ca^{2+}$  channels per  $Ca^{2+}$  release unit (CaRU) is in the physiological range. The Langevin description of stochastic  $Ca^{2+}$  release facilitates our investigation of correlations between successive puff/spark amplitudes, durations and inter-spark intervals, and how such puff/spark statistics depend on the number of channels per release site and the kinetics of  $Ca^{2+}$ -mediated inactivation of open channels. When  $Ca^{2+}$  inactivation/de-inactivation rates are intermediate—i.e., the termination of  $Ca^{2+}$  puff/sparks is caused by an increase in the number of inactivated channels—the correlation between successive puff/spark amplitudes is negative, while the correlations between puff/spark amplitudes and the duration of the preceding or subsequent inter-spark interval are positive. These correlations are significantly reduced or change signs when inactivation/de-inactivation rates are extreme (slow or fast) and puff/sparks terminate via stochastic attrition.

© 2015 Elsevier Inc. All rights reserved.

#### 1. Introduction

Intracellular Ca<sup>2+</sup> elevations known as Ca<sup>2+</sup> puffs and sparks [1,2] arise from the cooperative activity of inositol 1,4,5-trisphosphate receptors (IP<sub>3</sub>Rs) and ryanodine receptors (RyRs) that are clustered in Ca<sup>2+</sup> release units (CaRUs) on the endoplasmic reticulum/sarcoplasmic reticulum(ER/SR) membrane (see [3,4] for review). Single-channel Ca<sup>2+</sup> release events (Ca<sup>2+</sup> blips and quarks) are often observed as precursors to puffs, suggesting that these low-amplitude Ca<sup>2+</sup> release events trigger full-sized Ca<sup>2+</sup> puffs and sparks [5]. This is consistent with the observation that individual IP<sub>3</sub>Rs and RyRs are activated by cytosolic Ca<sup>2+</sup>, that is, small increases in [Ca<sup>2+</sup>] near these channels promotes further release of intracellular Ca<sup>2+</sup>, a process known as Ca<sup>2+</sup>-induced Ca<sup>2+</sup> release [6–9].

Although the activation mechanism of Ca<sup>2+</sup> puffs and sparks is agreed upon, the mechanism by which puffs and sparks terminate is understood to a lesser degree and may vary in different physiological contexts (see [10] for review). The short duration of most stochastic Ca<sup>2+</sup> release events (10–200 ms) suggests that puff/spark termina-

tion is facilitated by a robust negative feedback mechanism [1,11]. Because puff/sparks involve a finite number of channels, one possible termination mechanism is the simultaneous de-activation of all channels at a Ca<sup>2+</sup> release site, a phenomenon referred to as stochastic attrition [12,13]. Another possibility is that decreasing [Ca<sup>2+</sup>] in the SR/ER lumen reduces the driving force for Ca<sup>2+</sup> release and/or the contribution of feed-through Ca<sup>2+</sup>-activation to channel closure [14]. The inhibitory role of cytosolic Ca<sup>2+</sup>-mediated inactivation of IP<sub>3</sub>Rs and RyRs is also thought to contribute to puff/spark termination [10,15,16]. Termination of stochastic Ca<sup>2+</sup> release could also be mediated by state-dependent allosteric interactions between adjacent intercellular Ca<sup>2+</sup> channels [17], the redox state of IP<sub>3</sub>Rs and RyRs [18,19], and luminal regulation mediated by calsequestrin or other ER/SR proteins [20].

Discrete-state continuous-time Markov chains (CTMCs) are often used to model the stochastic gating of plasma membrane and intercellular ion channels, including clusters of IP<sub>3</sub>Rs and RyRs collectively gating within CaRUs [21]. These theoretical studies help clarify the factors that contribute to the generation and termination of Ca<sup>2+</sup> puffs and sparks. Simulations show that moderately fast Ca<sup>2+</sup> inactivation leads to puffs and sparks whose termination is facilitated by an increase in the number of inactivated channels during the puff/spark event, while slow Ca<sup>2+</sup> inactivation facilitates puff/spark termination due to stochastic attrition [12,22]. Ca<sup>2+</sup>-mediated coupling of IP<sub>3</sub>Rs

<sup>\*</sup> Corresponding author. Department of Applied Science, McGlothlin-Street Hall, Rm 312, The College of William and Mary, Williamsburg, VA 23187. Tel.: +1 757 603 1846. E-mail address: xwang06@email.wm.edu (X. Wang).

and RyRs also influences stochastic excitability of simulated CaRUs. The efficacy of this coupling is determined by the bulk ER/SR [Ca<sup>2+</sup>], the dynamics of luminal depletion, and the number, density and spatial arrangement of channels within a CaRU [23,24].

In this paper, we present a Langevin formulation of the stochastic dynamics of Ca<sup>2+</sup> release mediated by IP<sub>3</sub>Rs and RyRs that are instantaneously coupled through a local 'domain' Ca<sup>2+</sup> concentration (a function of the number of open channels). The Langevin approach assumes the number of Ca<sup>2+</sup> channels in individual CaRUs is large enough that the fraction of channels in different states can be treated as a continuous variable. Importantly, the computational efficiency of the Langevin approach is linear in the number of channel states and independent of the number of Ca<sup>2+</sup> channels per CaRU. This is quite distinct from compositionally defined Markov chain models, in which the number of CaRU states is exponential in the number of channel states and polynomial in the number of channels per CaRU. For this reason, the Langevin approach may be preferred for extensive parameter studies, provided the Langevin model of stochastic Ca<sup>2+</sup> release is a sufficiently good approximation to the corresponding Markov chain.

The remainder of this paper is organized as follows. Section 2 presents a continuous-time Markov chain model (and the corresponding Langevin formulation) of a CaRU composed of N three-state channels, each of which exhibits fast Ca<sup>2+</sup> activation and slower Ca<sup>2+</sup> inactivation. Section 3.1 uses the Langevin CaRU model to illustrate how the mechanism of spark termination depends on the rate of Ca<sup>2+</sup> inactivation. By comparing statistics of simulated puff/sparks (amplitude, duration and inter-event interval) generated by both models, Section 3.2 demonstrates that the Langevin description of the collective gating of Ca<sup>2+</sup> channels is indeed a good approximation to the corresponding Markov chain model when the number of Ca<sup>2+</sup> channels per release site is in the physiological range. Section 3.3 uses Langevin simulations of stochastic Ca<sup>2+</sup> release to perform an investigation of the correlations between successive puff/spark amplitudes, durations and inter-spark intervals and the dependence of these puff/spark statistics on the number of channels per release site and the kinetics of Ca<sup>2+</sup>-mediated inactivation of open channels.

## 2. Model formulation

# 2.1. Markov chain model of a Ca<sup>2+</sup> release site

The stochastic gating of intracellular channels is often modeled by discrete-state continuous-time Markov chains. For example, the following state and transition diagram,

$$\mathcal{C} \text{ (closed)} \overset{k_a^+ c'^0}{\underset{k_a^-}{\rightleftharpoons}} \mathcal{O} \text{ (open)} \overset{k_b^+ c'^0}{\underset{k_h^-}{\rightleftharpoons}} \mathcal{R} \text{ (refractory)}, \tag{1}$$

represents a minimal three-state channel that is both activated  $(\mathcal{C} \to \mathcal{O})$  and inactivated  $(\mathcal{O} \to \mathcal{R})$  by  $\operatorname{Ca}^{2+}$  [13]. In this diagram, c is the local [ $\operatorname{Ca}^{2+}$ ];  $\eta$  is the cooperativity of  $\operatorname{Ca}^{2+}$  binding;  $k_a^+ c^\eta, k_a^-, k_b^+ c^\eta$  and  $k_b^-$  are transition rates with units of time<sup>-1</sup>;  $k_a^+$  and  $k_b^+$  are association rate constants with units of concentration<sup>- $\eta$ </sup> time<sup>-1</sup>; and the dissociation constants for  $\operatorname{Ca}^{2+}$  binding are  $K_a^\eta = k_a^-/k_a^+$  and  $K_b^\eta = k_b^-/k_b^+$ . For simplicity, the cooperativity of  $\operatorname{Ca}^{2+}$  binding is the same for the activation and inactivation processes  $(\eta = 2)$ .

It is straightforward to construct a  $Ca^{2+}$  release unit (CaRU) model that includes an arbitrary number N of stochastically gating three-state channels. Because the channels are identical, such a model has (N+2)(N+1)/2 distinguishable states that may be enumerated as follows,

$$(N, 0, 0)$$
  $(N-1, 1, 0)...(0, 1, N-1)$   $(0, 0, N),$  (2)

where each state takes the form  $(N_C, N_O, N_R)$  and  $N_C, N_O$  and  $N_R$  are the number of channels in closed, open and refractory states,

respectively. For example, let us assume that when  $N_{\mathcal{O}} = n$ , the local  $[\mathsf{Ca}^{2+}]$  experienced by channels in the CaRU is given by

$$c_n = c_\infty + nc_*, \tag{3}$$

where  $c_{\infty}$  is the bulk [Ca<sup>2+</sup>]. We will refer to the parameter  $c_*$  as the coupling strength, because this parameter determines the increment in local [Ca<sup>2+</sup>] that occurs when an individual Ca<sup>2+</sup> channel opens. The transition rates for the compositionally defined Markov chain model with state space given by Eq. (2) are each the product of a transition rate of the single channel model (Eq. (1)) and the number of channels that may make that transition. For example, in a release site composed of 20 channels, the transition rates out of the state (15,3,2) would be  $15k_a^+c_3^\eta=15k_a^+(c_\infty+3c_*)^\eta, 3k_a^-, 3k_b^+c_3^\eta=3k_b^+(c_\infty+3c_*)^\eta$ , and  $2k_b^-$  respectively, with destination states (14,4,2), (16,2,2), (15,2,3) and (15,4,1).

#### 2.2. The Langevin description of a Ca<sup>2+</sup> release site

A Langevin description of the CaRU is an alternative to the Markov chain model presented above [25,26]. The Langevin approach assumes that the number of channels in the CaRU is large enough so that the fraction of channels in each state can be treated as continuous randomly fluctuating variables that solve a stochastic differential equation (SDE) system. For example, the Langevin equation of a CaRU composed of *N* three-state channels (Eq. (1)) is given by [27]

$$\frac{d\mathbf{f}}{dt} = \mathbf{f}Q + \mathbf{\xi}(t),\tag{4}$$

where f is a row vector of the fraction of channels in each state,  $f = (f_C, f_C, f_R)$ , Q is the infinitesimal generator matrix (Q-matrix) given by

$$Q = (q_{ij}) = \begin{pmatrix} \diamondsuit & k_a^+ c^{\eta} & 0 \\ k_a^- & \diamondsuit & k_b^+ c^{\eta} \\ 0 & k_b^- & \diamondsuit \end{pmatrix}, \tag{5}$$

where the local [Ca<sup>2+</sup>] can be written as  $c=c_{\infty}+f_{\mathcal{O}}\bar{c}$  with  $\bar{c}=Nc_*$ , the off-diagonal elements are transition rates  $(q_{ij}\geq 0)$ , and the diagonal elements ( $\bullet$ ) are such that each row sums to zero,  $q_{ii}=-\Sigma_{j\neq i}\,q_{ij}<0$ . In Eq. (4),  $\xi(t)=(\xi_{\mathcal{C}}(t),\xi_{\mathcal{O}}(t),\xi_{\mathcal{R}}(t))$  is a row vector of rapidly varying forcing functions with mean zero,

$$\langle \boldsymbol{\xi}(t) \rangle = \mathbf{0},\tag{6}$$

and two-time covariance,

$$\langle \boldsymbol{\xi}(t)^T \boldsymbol{\xi}(t') \rangle = \Gamma(\boldsymbol{f}) \delta(t - t'), \tag{7}$$

where  $\Gamma(\mathbf{f}) = (\gamma_{ij})$  and

$$\gamma_{ij} = -\frac{(q_{ij}f_i + q_{ji}f_j)}{N} \ (i \neq j)$$
(8)

$$\gamma_{ii} = -\sum_{i \neq i} \gamma_{ij}. \tag{9}$$

The Langevin model is simulated by integrating Eqs. (4)–(9) using a modification of the Euler-Maruyama method [28], appropriate for a stochastic ODE with dependent variables constrained to the unit interval, i.e.,  $0 \le f_i \le 1$  (see Wang et al. [29] for details).

## 3. Results

The focus of this paper is a theoretical analysis of spark statistics such as puff/spark duration, amplitude and inter-event interval. We are specifically interested in the relationship between successive puff/spark amplitudes, whether puff/sparks and inter-event intervals are positively or negatively correlated, and how such puff/spark

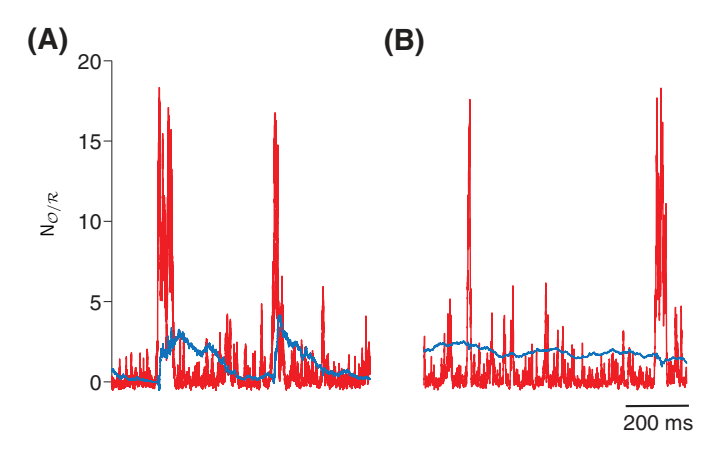


**Fig. 1.** The number of open channels ( $N_{\mathcal{O}}$ , red) and refractory channels ( $N_{\mathcal{R}}$ , blue line) during simulated Ca<sup>2+</sup> puffs/sparks obtained by numerically integrating the Langevin model (Eqs. (4)–(9)) with integration time step  $\Delta t=0.1\,$  ms). Ca<sup>2+</sup>-inactivation/de-inactivation rates are 10-fold slower in B ( $k_b^+=0.0015\,\mu M^{-\eta}\, {\rm ms}^{-1}, k_b^-=0.0005\, {\rm ms}^{-1}$ ) than A ( $k_b^+=0.015\,\mu M^{-\eta}\, {\rm ms}^{-1}, k_b^-=0.005\, {\rm ms}^{-1}$ ). Other parameters:  $k_a^+=1.5\,\mu M^{-\eta}\, {\rm ms}^{-1}, k_a^-=0.5\, {\rm ms}^{-1}, c_*=0.06\, \mu M, \, c_\infty=0.05\, \mu M, \, \eta=2, \, K_a=K_b=0.58\, \mu M$ . (For interpretation of the references to color in this figure legend, the reader is referred to the web version of this article.)

statistics depend on the single channel kinetics (e.g., Ca<sup>2+</sup> inactivation rate). The Langevin approach to modeling CaRU dynamics facilities the large number of Monte Carlo simulations required for this analysis. Below we will first show representative Langevin simulation and illustrate how sequences of spark amplitudes, durations, and inter-event intervals are obtained from Langevin release site simulation (Section 3.1). Next we validate the Langevin release site model by comparing the statistics of simulated puff/sparks (amplitude, duration and inter-event interval) generated by the Langevin model and the corresponding Markov chain model (Section 3.2). This is followed by an analysis of correlations between successive puff/spark amplitudes, durations and inter-spark intervals, and how such puff/spark statistics depend on the number of channels per release site and the kinetics of Ca<sup>2+</sup>-mediated inactivation of open channels (Section 3.3).

#### 3.1. Representative Langevin simulations

In prior work, Groff and Smith [13] found that Ca<sup>2+</sup>-dependent inactivation may facilitate puff/spark termination in two distinct ways depending on Ca<sup>2+</sup>-inactivation rates. Fig. 1A and B use the Langevin model (Eqs. (4)-(9)) to illustrate these two different termination mechanisms. In Fig. 1A the number of inactivated channels ( $N_R$ , blue line) increases during each puff/spark event, and decreases during the inter-event intervals between puff/sparks. In this case, the Ca<sup>2+</sup> inactivation rate is such that the accumulation of inactivated channels results in puff/spark termination. In Fig. 1B, the Ca<sup>2+</sup> inactivation/deinactivation rates are reduced by 10-fold compared with that of Fig. 1A. In this case the number of inactivated channels ( $N_R$ , blue line) is relatively constant; consequently, the CaRU composed of N threestate channels effectively reduces to a collection of  $N-N_R$  two-state channels. In Fig. 1B, the puff/spark termination is due to stochastic attrition [10,30], that is, the coincident de-activation  $(N_{\mathcal{O}} \to N_{\mathcal{C}})$  of all channels in the CaRU that are not in the refractory state  $N_R$  [13].

Fig. 2A shows a Langevin simulation of the fraction of open channels,  $f_{\mathcal{O}}$ , for a CaRU composed of 20 three-state Ca<sup>2+</sup> channels. The duration of the ith Ca<sup>2+</sup> release event ( $D_i$ ) is the time elapsed between the first channel opening (up arrows) and the last channel closing (down arrows) of each simulated spark. Because the fraction of open channels in the Langevin description is continuous (as opposed to discrete), the first/last channel opening is defined as  $f_{\mathcal{O}}$  crossing the threshold (1/N, dashed line) in the upward/downward direction (vertical arrows). The amplitude of ith Ca<sup>2+</sup> release event ( $A_i$ ) is defined

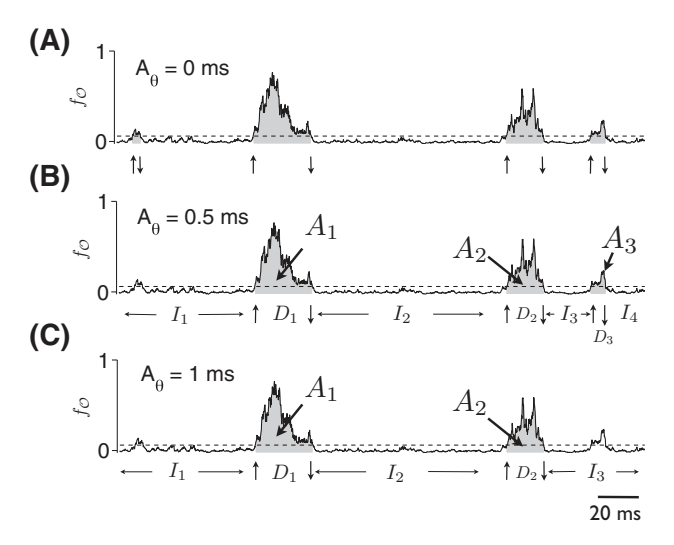


**Fig. 2.** The puff/spark detectability threshold  $A_{\theta}$  eliminates small Ca<sup>2+</sup> release events from the correlation analysis of the sequence of simulated spark amplitudes, durations and inter-event intervals. A: 20 three-state Ca<sup>2+</sup> channels simulated using the Langevin approach (Eqs. (4)–(9)). The fraction of open channels,  $f_{\mathcal{O}}$ , is shown as a function of time. The dashed line denotes  $f_{\mathcal{O}}=1/N$ , the threshold for identifying Ca<sup>2+</sup> release events. Up and down arrows indicate crossings that define the beginning and ending of Ca<sup>2+</sup> sparks. B: For an amplitude threshold  $A_{\theta}=0.5$  ms, the first Ca<sup>2+</sup> release event in A is discarded and three Ca<sup>2+</sup> spark events are considered detectable. C: For  $A_{\theta}=1$  ms, the first and last Ca<sup>2+</sup> release event in A are discarded, and two Ca<sup>2+</sup> spark events are detectable.

as the integrated area under  $f_{\mathcal{O}}(t)$  during the release event (gray). The inter-event interval  $(I_i)$  is the length of time between the (i-1)th and ith  $Ca^{2+}$  release events. Because in experimental studies many  $Ca^{2+}$  release events may be too small for detection, we specify an amplitude threshold,  $A_{\theta}$ , and only the events with greater amplitude  $(A_i \geq A_{\theta})$  are used in the calculation of spark statistics. For example, using an amplitude threshold of  $A_{\theta}=0.5$  ms, only three of four events are of sufficient magnitude to be included in the sequence of puff/spark durations, amplitudes and inter-event intervals chosen for further analysis (Fig. 2B). If  $A_{\theta}=1$  ms, only two of the four events are included (Fig. 2C).

# 3.2. Validation of Langevin approach

Using CaRUs composed of N = 20 three-state channels and amplitude threshold of  $A_{\theta} = 1$  ms (lower dashed line) that filters out small events, Fig. 3A shows a strong linear relationship between spark amplitudes and durations in both Markov chain (o) and Langevin (+) simulations. The linear amplitude-duration relationship calculated via the Markov chain model becomes less significant for small release events ( $A_{\theta} \leq 0.1$  ms). This indicates that the Langevin simulation may not agree with the Markov chain simulation for small release events. However, these events are experimentally undetectable. We therefore are more interested in the data where small release events are filtered out. Using  $A_{\theta} = 1$  or 2 ms, Fig. 3B-D compares the cumulative distribution functions of spark amplitude (B), duration (C) and inter-event interval (D) for CaRUs composed of 20 (thin) and 60 (thick lines) three-state channels. In these simulations, the aggregate coupling strength  $\bar{c} = Nc_*$  is fixed, as opposed to fixing the contribution to the local [Ca<sup>2+</sup>] made by a single open channel  $(c_*)$ . The spark duration and inter-event interval distributions move to the right as the number of channels increases (Fig. 3C-D), that is, for larger N, spark durations and inter-event intervals are typically longer. At the same time, increasing N leads to sparks that on average have smaller amplitudes (Fig. 3B). For high amplitude threshold  $A_{\theta}$ , the distributions move to the right because smaller events are filtered out. Most importantly, the agreement between Markov chain (pink solid) and

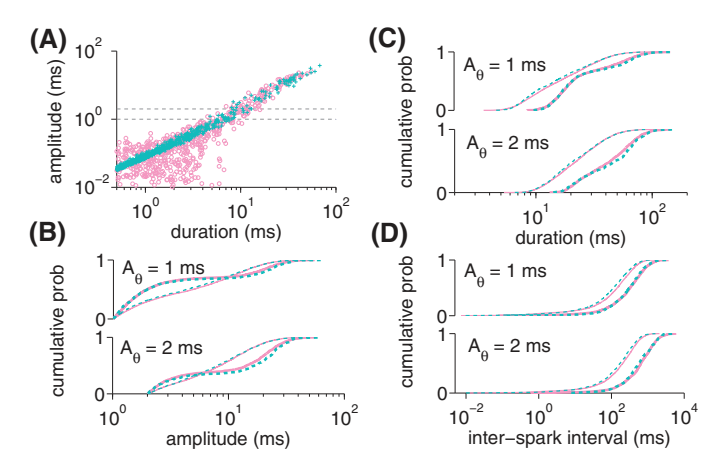


**Fig. 3.** Spark duration, amplitude and inter-event interval statistics. A: Scatter plot of spark amplitude vs. duration in 20-channel Langevin (+) and Markov chain ( $\circ$ ) simulations shows a strong linear dependence for durations greater than 1 ms. After filtering out small amplitude release events ( $A_{\theta} \leq 1$  ms, lower dashed line), a linear regression of the amplitude (a) and duration (d) scatter plot yields a = -2.51 + 0.49d (Langevin,  $r^2 = 0.95$ ) and a = -2.68 + 0.50d (Markov chain,  $r^2 = 0.94$ , regression lines not shown). B–D: The cumulative probability distributions of spark amplitude, duration and inter-event interval in Langevin (blue dashed) and Markov chain (pink solid lines) simulations for amplitude thresholds  $A_{\theta} = 1$  and 2 ms, respectively (dashed lines in panel A). Parameters as in Fig. 1A with  $\bar{c} = 1.2 \ \mu M$  and N = 20 or 60 (thin and thick lines, respectively). (For interpretation of the references to color in this figure legend, the reader is referred to the web version of this article.)

Langevin (blue dashed line) calculations of sparks statistics shown in Fig. 3B–D validates our use of Langevin approach for further analysis.

#### 3.3. Analysis of spark statistics

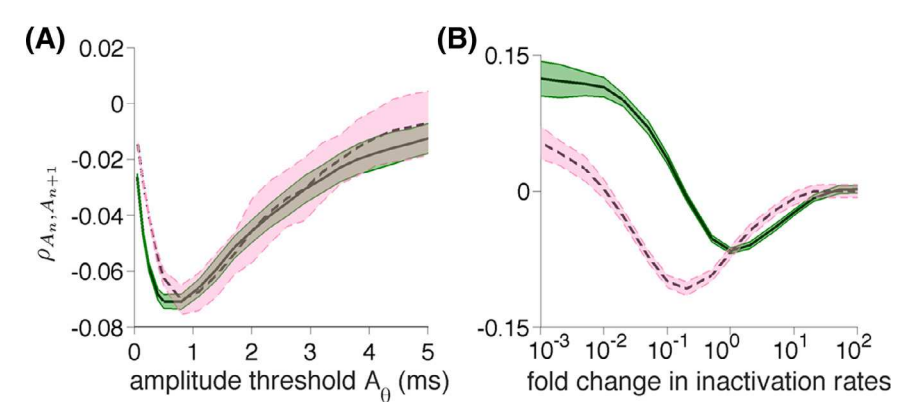
Our analysis of puff/sparks statistics begins with Fig. 4A which shows the Pearson correlation coefficient between successive puff/spark amplitudes,  $\rho_{A_n,A_{n+1}}$ , when the standard parameters for Ca^2+-inactivation and de-inactivation are used (as in Fig. 1A, where sparks terminate through the accumulation of inactivated channels). The correlation between successive puff/spark amplitudes is small but negative regardless of the amplitude threshold ( $A_{\theta}$ ), indicating event-to-event alternation of puff/spark amplitude (small, large, small, large, etc.). The alternation in puff/spark amplitudes is most pronounced (i.e., the correlation is most negative) when  $A_{\theta}$  is about 0.5 ms for N=20 channels and 1 ms for 60 channels.

Fig. 4B shows how this tendency toward alternating puff/spark amplitude depends on the rate of  $Ca^{2+}$  inactivation/de-inactivation (with dissociation constant  $K_b$  fixed). Using an amplitude threshold

of  $A_{\theta}=1$  ms, a negative correlation between successive puff/spark amplitudes is observed for intermediate inactivation rates (for both 20 and 60 channels). This negative correlation occurs because large puff/sparks terminate with a relatively large fraction of inactivated channels (cf. Fig. 1A). Consequently, fewer channels are available to participate the next (small amplitude)  $\text{Ca}^{2+}$  release event. Conversely, small puff/sparks terminate with fewer  $\text{Ca}^{2+}$ -inactivated channels, and the subsequent puff/spark amplitudes are thus likely to be larger. Negative amplitude–amplitude correlation is not observed when the inactivation rates are reduced or increased by 100-fold compared to the standard parameters. Interestingly, for a larger number of channels (N=60), the most pronounced amplitude alternation is larger in magnitude (i.e., a stronger negative correlation) and occurs at slower inactivation rates than the N=20 case.

When the inactivation rate is slow enough that the number of refractory channels  $N_R$  does not change dramatically during the active phase of any individual puff/spark event, the mechanism that may generate negative amplitude-amplitude correlation is no longer operative, because  $A_n$  does not affect  $N_R$  at puff/spark termination. Similarly, when the inactivation rates are very fast,  $A_n$  cannot influence  $N_R$  at spark termination because  $N_R$  is in quasistatic equilibrium with  $N_{\mathcal{O}}$  ( $N_{\mathcal{R}}=k_{h}^{+}c^{\eta}/k_{h}^{-}$ ). For both very slow and very fast inactivation rates, stochastic attrition is the mechanism of spark termination and, consequently, spark amplitudes are less negatively correlated and may even be positive. The positive amplitude-amplitude correlation that is observed at slow inactivation/de-inactivation rates is due to the auto-correlation time of  $N_R$  surpassing the typical interevent interval duration. This leads to sequences of multiple small amplitude events (when  $N_R$  is greater than average) and multiple large amplitude events (when  $N_R$  is less than average). This effect is greater for 20 channels than 60, consistent with smaller inter-event interval durations observed in the 20-channel case (see Fig. 3D).

Fig. 5 is similar in structure to Fig. 4, but focuses on the correlation between inter-event intervals and the subsequent puff/spark amplitudes,  $\rho_{I_n,A_n}$ , which are positively correlated regardless of amplitude threshold  $A_{\theta}$  (Fig. 5A). Following a long inter-event interval, the channels that were inactivated at the end of the preceding puff/spark are more likely to be available for the subsequent  $Ca^{2+}$  release event. Consequently, the spark amplitudes following long quiescent periods tends to be larger than those that follow brief quiescent periods. Fig. 5B shows that the interval-amplitude correlation becomes less positive or even negative for sufficiently slow or fast inactivation rates. Similarly, Fig. 6A shows a small positive correlation between puff/spark amplitudes and the subsequent inter-event intervals ( $\rho_{A_n,I_{n+1}}$ ). Fig. 6B shows that this amplitude-interval correlation is less positive or even negative for sufficiently fast or slow inactivation rates (similar to the interval-amplitude correlation of Fig. 5B).



**Fig. 4.** Correlation between successive puff/spark amplitude ( $\rho_{A_0,A_{n+1}}$ ). A: Correlation as a function of amplitude threshold  $A_\theta$ . B: Using  $A_\theta=1$  ms, the correlation as a function of the fold change in inactivation and de-inactivation rates for fixed dissociation constant. In (A) and (B), the mean (thick curve) +/— one standard deviation (shaded region) over 10 simulations (each 8000 s) is shown. Parameters as in Fig. 1A with N=20 (solid) and 60 (dashed lines) and  $\bar{c}=1.2~\mu$ M.

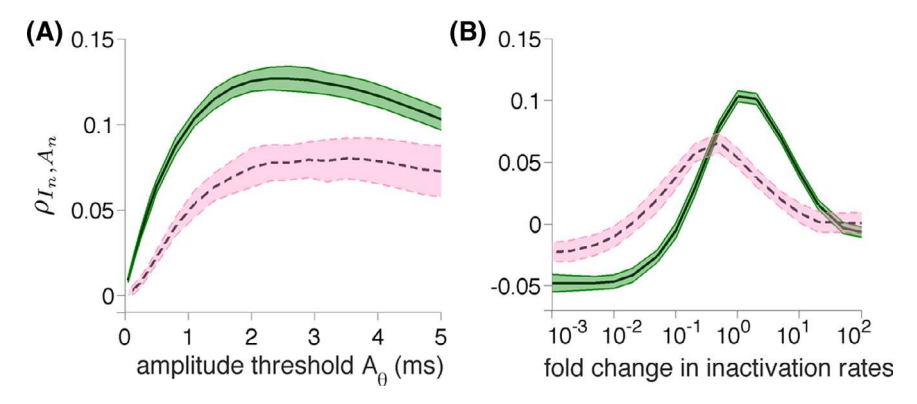


**Fig. 5.** Correlation between inter-spark interval and subsequent puff/spark amplitude ( $\rho_{l_n, A_n}$ ). A: Correlation as a function of amplitude threshold  $A_{\theta}$ . B: Using  $A_{\theta} = 1$  ms, the correlation as a function of the fold change in inactivation/de-inactivation rates for fixed dissociation constant. See Fig. 4 legend.

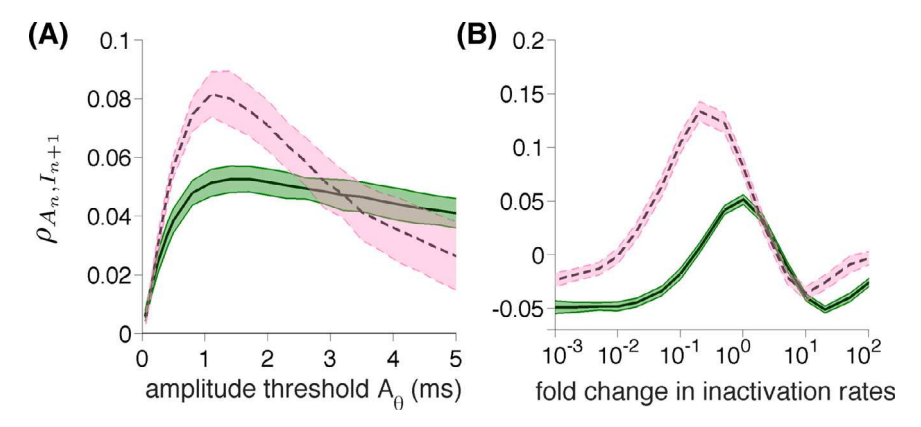


**Fig. 6.** Correlation between puff/spark amplitude and subsequent inter-spark interval  $(\rho_{A_n,I_{n+1}})$ . A: Correlation as a function of amplitude threshold  $A_{\theta}$ . B: Using  $A_{\theta}=1$  ms, the correlation as a function of the fold change in inactivation/de-inactivation rates for fixed dissociation constant. See Fig. 4 legend.

# 4. Discussion

This paper presents a Ca<sup>2+</sup> release unit (CaRU) modeling approach based on a Langevin description of stochastic Ca<sup>2+</sup> release. This Langevin model facilitates our investigation of correlations between successive puff/spark amplitudes and inter-spark intervals, and how such puff/spark statistics depend on the number of channels per release site and the kinetics of Ca<sup>2+</sup>-mediated inactivation of open channels. We find that when Ca<sup>2+</sup> inactivation/de-inactivation rates are intermediate—i.e., the termination of Ca<sup>2+</sup> puff/sparks is caused by an increase in the number of inactivated channels—the correlation between successive puff/spark amplitudes is negative, while the correlations between puff/spark amplitudes and the duration of the preceding or subsequent inter-spark interval are positive. These correlations are significantly reduced or change sign when inactivation/de-inactivation rates are extreme (slow or fast), that is, when puff/sparks terminate via stochastic attrition.

# 4.1. Comparison to experiment

Puff/spark amplitudes, durations and inter-event intervals have been extensively studied in recent years [2,31–35]. Positive correlations between spark amplitude and duration [31] and rise time [36] have been observed. The rise time of spark fluorescence is interpreted as a proxy for the duration of  $Ca^{2+}$  release during the spark. Spark amplitude in our release site simulations is an increasing function of spark duration (i.e., positively correlated, with  $r^2 = 0.95$ ).

This positive correlation is not always observed in experimental [37] and theoretical work [33]. Shen et al. [34] suggest that spark amplitude is independent of rise time, but is strongly and positively related to the mean or maximal rising rate. Their results show that

spark rising time is negatively related to the mean rising rate, suggesting that the regulation of Ca<sup>2+</sup> termination is a negative feedback and the strength of which is proportional to the ongoing release flux or the number of activated RyRs [34]. In contrast to prior experimental results [36], the amplitude-rising time relationship is negative in the simulation work presented by Stern et al. [38], because a long rise time implies a slower release of approximately the same amount of junctional SR Ca<sup>2+</sup>.

In our simulations, successive puff/spark amplitudes are negatively correlated, but only weakly (the peak is less than 0.15). This is consistent with experimental measurements of the correlation between successive puff amplitude were not statistically significant [39].

Inter-event intervals are determined both by recovery from a refractory state established by the preceding puff/spark, and a stochastic triggering which leads to an exponential distribution at longer intervals [2,40]. The histograms of inter-puff interval measured at individual puff site show an initial increase of the inter-puff interval distribution, which is compatible with recovery from a negative feedback occurring during the puff [41]. In ventricular myocytes, Sobie et al. [42] found that the relative amplitude of the second spark tends to be small when the spark-to-spark delay is short and larger as this delay increases. Moreover, Fraiman et al. [16] observed that in Xenopus oocytes, puffs of large amplitudes tend to be followed by a long inter-puff time, and puffs that occur after a large inter-puff time are most likely large. One possible explanation of this positive interval-amplitude and amplitude-interval correlation is that high cytosolic [Ca<sup>2+</sup>] attained during a puff/spark inhibits channels within the CaRU, so that the amplitude and probability of occurrence of a subsequent puff recover with a long time course [16]. Another possible mechanism is local Ca<sup>2+</sup> depletion of ER lumen leading to decreased channel open probability [43]. Parker and Wier [40] studied the relationship between the preceding inter-spark interval and the amplitude peak of the spark at the end of the interval and found no correlation. Our simulations exhibit both negative and positive values of  $\rho_{I_n,A_n}$  and  $\rho_{A_n,I_{n+1}}$ , but when ranging over inactivation/de-inactivate rates the most positive value observed was always less than 0.2.

#### 4.2. Comparison to prior theoretical work

Several types of modeling approaches based on microscopic kinetics of channels have been developed to study puff/spark statistics. For example, using a simplification of the Sneyd–Dufour IP<sub>3</sub>R model, Ullah and Jung observed that simulated puff amplitudes and lifetime are positively correlated ( $\rho=0.31$ ) [35,44].

Ullah et al. [45] presented a model of  $IP_3R$  derived directly from single channel patch clamp data. Their results suggest that puff terminations is due to self-inhibition rather than  $ER Ca^{2+}$  depletion (unlike cardiac muscle, where local SR depletion is important for spark termination [46]).

Stern et al. [38] utilized a simplified, deterministic model of cardiac myocyte couplon dynamics to show that spark metastability depends on the kinetic relationship of RyR gating and junctional SR refilling rates. They found that spark amplitudes is negatively correlated to rise time, in spite of the fact that positive correlation between amplitudes and rise time was observed in chemically skinned cat atrial myocytes [36].

Some prior work utilizing the Langevin formulation to investigate puff statistics has focused on a reduced Hodgkin–Huxley-like IP<sub>3</sub> receptor model in which noise terms were added to the gating variable [33,47,48]. By comparing Langevin and Markov chain simulations, they determined that Langevin approach yields more puffs with larger amplitudes, which leads to a drop-off of distribution at smaller amplitude; we did not observe this discrepancy in our Langevin simulation. Jung and co-workers also investigated the correlation between puff amplitude and lifetime and found that the correlation values are typically smaller than 0.3 [33].

#### 4.3. Advantages and limitations of the Langevin approach

While the Markov chain and Langevin approaches lead to similar results, the runtimes for Langevin simulations is often shorter. One expects Markov chain simulation runtimes to be proportional to the number of CaRU states, a quantity that is exponential in the number of distinct channel states. To see this, consider a CaRU composed of N identical M-state channels, the number of distinguishable CaRU states is given by (N + M - 1)!/[N!(M - 1)!]. For example, for 20, 60, and 100 identical three-state channels, there are 231, 1891, and 5151 distinguishable states, respectively. Conversely, Langevin simulation runtimes such as those presented in this study are independent of the number of channels (i.e., N is a model parameter) and proportional to the number of states M. Table 1 illustrates this by comparing the simulation time of the Markov chain and the Langevin release site calculations shown here. The runtime of the Markov chain model increases significantly as the number of channels per release site N increases, while the simulation time of Langevin description is inde-

The Langevin formulation presented here is applicable and efficient when the number of channels per release site is large enough so that the fraction of channels in each state can be treated as a continuous variable. When this condition is not met, the use of Markov chain simulation or the slightly less-restrictive  $\tau$ -leaping approach may be more appropriate [28].

This study has focused on correlations between spark statistics using relatively restrictive modeling assumptions, including a minimal three-state channel model and instantaneous coupling of channels.

**Table 1** Simulation time of a CaRU composed of *N* three-state channels, where *N* is 20, 60 and 100 respectively. Time step  $\Delta t$  is 0.1 or 0.01 ms. The reported simulation times are the average of 10 100 s trials. Parameters as in Fig. 1A.

Model	Simulation time (s)	Standard deviation (s)
Markov chain $(N = 20)$	11.78	0.56
Markov chain $(N = 60)$	148.86	2.37
Markov chain ( $N = 100$ )	416.80	4,26
Langevin ( $N = 20$ , $\Delta t = 0.1$ ms)	4.38	0.32
Langevin ( $N = 60$ , $\Delta t = 0.1$ ms)	4.28	0.35
Langevin ( $N = 100$ , $\Delta t = 0.1$ ms)	4.30	0.36
Langevin ( $N = 20$ , $\Delta t = 0.01$ ms)	43.98	3.14
Langevin ( $N = 60$ , $\Delta t = 0.01$ ms)	43.26	3.89
Langevin ( $N = 100$ , $\Delta t = 0.01$ ms)	44.47	3.52

One important observation is that correlations between the amplitude, duration, and interval-event intervals of simulated Ca<sup>2+</sup> puffs and sparks are strongly influenced by spark termination mechanism (i.e., Ca<sup>2+</sup>-dependent inactivation or stochastic attrition-like). While the statistical correlations between puff/spark amplitude, duration and inter-event interval are likely to be model dependent, it straightforward to extend the Langevin approach used in this paper to channel models of arbitrary complexity (see Eqs. (8)–(9)). The Langevin formulation can also be extended to account for luminal depletion and/or regulation, both of which are known to influence spark termination [14]. The relationship between spark statistics and Ca<sup>2+</sup> homeostasis can be studied by coupling Langevin release site models to balance equations for the bulk myoplasmic and network SR [Ca<sup>2+</sup>] [29]. The Langevin approach can also be used to analyze the effect of Ca<sup>2+</sup> buffers on fluctuations in Ca<sup>2+</sup> concentration [49].

Because we assume mean-field coupling, the Langevin approach presented here is not well-suited to investigate how puffs and sparks may depend on release site ultrastructure, i.e., the spatial location of channels within individual release units [24]. On the other hand, simulations of stochastic propagating Ca<sup>2+</sup> waves and cell-wide spatial phenomena such as Ca<sup>2+</sup> alternans could be constructed using Langevin representations of multiple interacting release sites distributed throughout the cytosolic milieu.

# Acknowledgments

The work was supported in part by National Science Foundation Grant DMS 1121606 to GDS and the Biomathematics Initiative at The College of William & Mary.

### References

- H. Cheng, W.J. Lederer, M.B. Cannell, Calcium sparks: elementary events underlying excitation-contraction coupling in heart muscle, Science 262 (5134) (1993) 740–744.
- [2] Y. Yao, J. Choi, I. Parker, Quantal puffs of intracellular Ca<sup>2+</sup> evoked by inositol trisphosphate in Xenopus oocytes, J. Physiol. 482 (Pt 3) (1995) 533–553.
- [3] M.J. Berridge, Cell signalling. a tale of two messengers., Nature 365 (6445) (1993)
- [4] D.M. Bers, Cardiac excitation-contraction coupling, Nature 415 (6868) (2002) 198–205.
- [5] H.J. Rose, S. Dargan, J.W. Shuai, I. Parker, 'Trigger' events precede calcium puffs in Xenopus oocytes, Biophys. J. 91 (11) (2006) 4024–4032.
- [6] I. Bezprozvanny, J. Watras, B.E. Ehrlich, Bell-shaped Ca<sup>2+</sup>-response curves of Ins(1,4,5)P3- and Ca<sup>2+</sup>-gated channels from endoplasmic reticulum of cerebellum, Nature 351 (6329) (1991) 751–754.
- [7] E.A. Finch, T.J. Turner, S.M. Goldin, Calcium as a coagonist of inositol 1,4,5-trisphosphate-induced calcium release, Science 252 (5004) (1991) 443–446.
- [8] I. Parker, Y. Yao, Ca<sup>2+</sup> transients associated with openings of inositol trisphosphate-gated channels in Xenopus oocytes, J. Physiol. 491 (Pt 3) (1996) 663–668.
- [9] I. Parker, J. Choi, Y. Yao, Elementary events of IP<sub>3</sub>-induced Ca<sup>2+</sup> liberation in Xenopus oocytes: hot spots, puffs and blips, Cell Calcium 20 (2) (1996) 105–121.
- [10] M.D. Stern, H. Cheng, Putting out the fire: what terminates calcium-induced calcium release in cardiac muscle? Cell Calcium 35 (6) (2004) 591–601.
- [11] E. Niggli, N. Shirokova, A guide to sparkology: the taxonomy of elementary cellular Ca<sup>2+space</sup> signaling events, Cell Calcium 42 (4–5) (2007) 379–387.

- [12] H. DeRemigio, G.D. Smith, The dynamics of stochastic attrition viewed as an absorption time on a terminating Markov chain, Cell Calcium 38 (2) (2005) 73-86.
- [13] J.R. Groff, G.D. Smith, Calcium-dependent inactivation and the dynamics of calcium puffs and sparks, J. Theor. Biol. 253 (3) (2008) 483–499.
- M.A. Huertas, G.D. Smith, The dynamics of luminal depletion and the stochastic gating of Ca<sup>2+</sup>-activated Ca<sup>2+</sup> channels and release sites., J. Theor. Biol. 246 (2) (2007) 332–354.
- M. Fill. Mechanisms that turn-off intracellular calcium release channels. Front. Biosci, 8 (2002) d46-d54.
- [16] D. Fraiman, B. Pando, S. Dargan, I. Parker, S.P. Dawson, Analysis of puff dynamics in oocvtes: interdependence of puff amplitude and interpuff interval, Biophys. J. 90 (11) (2006) 3897–3907.
- S.M. Wiltgen, G.D. Dickinson, D. Swaminathan, I. Parker, Termination of calcium puffs and coupled closings of inositol trisphosphate receptor channels, Cell Calcium 56 (3) (2014) 157-168
- [18] A.V. Zima, L.A. Blatter, Redox regulation of cardiac calcium channels and transporters, Cardiovas. Res. 71 (2006) 310-321.
- [19] L.C. Hool, B. Corry, Redox control of calcium channels: from mechanisms to therapeutic opportunities, Antioxid. Redox Signal. 9 (4) (2007) 409-435.
- [20] I. Györke, N. Hester, L.R. Jones, S. Györke, The role of calsequestrin, triadin, and junctin in conferring cardiac ryanodine receptor responsiveness to luminal calcium, Biophys. J. 86 (4) (2004) 2121–2128.
- [21] J.R. Groff, H. DeRemigio, G.D. Smith, Markov chain models of ion channels and the collective gating of Ca<sup>2+</sup> release sites., in: C. Laing, L. Gabriel (Eds.), Stochastic Methods in Neuroscience, Oxford University Press, 2010, pp. 29-64.
- [22] J.R. Groff, G.D. Smith, Ryanodine receptor allosteric coupling and the dynamics of calcium sparks, Biophys. J. 95 (1) (2008) 135–154.
- [23] V. Nguyen, R. Mathias, G.D. Smith, A stochastic automata network descriptor for markov chain models of instantaneously-coupled intracellular Ca<sup>2+</sup> channels, Bull. Math. Biol. 67 (3) (2005) 393-432.
- [24] H. DeRemigio, G.D. Smith, Calcium release site ultrastructure and the dynamics of puffs and sparks, Math. Med. and Biol. 25 (1) (2008) 65-85.
- C.W. Gardiner, Handbook of Stochastic Methods for Physics, Chemistry and the Natural Science, Springer, 1985.
- C.E. Dangerfield, D. Kay, K. Burrage, Modeling ion channel dynamics through reflected stochastic differential equation, Phys. Rev. E 85 (2012) 051907.
- J.E. Keizer, Statistical Thermodynamics of Nonequilibrium Processes, Springer Verlag, Berlin, 1987.
- [28] D.T. Gillespie, The chemical Langevin equation, J. Chem. Phys. 113 (1) (2000) 297-306.
- X. Wang, S. Weinberg, Y. Hao, E.A. Sobie, G.D. Smith, Calcium homeostasis in a local/global whole cell model of permeabilized ventricular myocytes with a langevin description of stochastic calcium release, Am. J. Physiol. Heart Cir. Physiol. 308 (5) (2015) H510-H523. doi: http://dx.doi.org/10.1152/ajpheart.00296.2014.
- [30] M.D. Stern, Theory of excitation-contraction coupling in cardiac muscle, Biophys. J. 63 (2) (1992) 497-517.
- H. Cheng, L.S. Song, N. Shirokova, A. González, E.G. Lakatta, E. Ríos, M.D. Stern, Amplitude distribution of calcium sparks in confocal images: theory and studies with an automatic detection method, Biophys. J. 76 (2) (1999) 606-617.

- [32] E. Ríos, N. Shirokova, W.G. Kirsch, G. Pizarro, M.D. Stern, H. Cheng, A. Gonzalez, A preferred amplitude of Ca<sup>2+</sup> sparks in skeletal muscle, Biophys. J. 80 (1) (2001) 169-183.
- [33] J.W. Shuai, P. Jung, Stochastic properties of Ca<sup>2+</sup> release of inositol 1,4,5trisphosphate receptor clusters, Biophys. J. 83 (1) (2002) 87-97.
- [34] J. Shen, S. Wang, L. Song, T. Han, H. Cheng, Polymorphism of Ca<sup>2+</sup> sparks evoked from in-focus Ca<sup>2+</sup> release units in cardiac myocytes, Biophys. J. 86 (1)(Pt 1) (2004) 182-190.
- [35] G. Ullah, P. Jung, Modeling the statistics of elementary calcium release events, Biophys. J. 90 (10) (2006) 3485-3495.
- [36] V.M. Shkryl, L.A. Blatter, E. Ríos, Properties of Ca<sup>2+</sup> sparks revealed by fourdimensional confocal imaging of cardiac muscle, J. Gen. Physiol. 139 (3) (2012) 189-207
- [37] S. Wang, L. Song, L. Xu, G. Meissner, E.G. Lakatta, E. Ríos, M.D. Stern, H. Cheng, Thermodynamically irreversible gating of ryanodine receptors in situ revealed by stereotyped duration of release in Ca<sup>2+space</sup>sparks, Biophys. J. 83 (1) (2002) 242-251.
- [38] M.D. Stern, E. Ríos, V.A. Maltsey, Life and death of a cardiac calcium spark, J. Gen. Physiol. 142 (3) (2013) 257-274.
- [39] N. Callamaras, I. Parker, Phasic characteristic of elementary Ca<sup>2+</sup> release sites underlies quantal responses to IP3, EMBO J. 19 (14) (2000) 3608-3617
- [40] I. Parker, W.G. Wier, Variability in frequency and characteristics of Ca<sup>2+</sup> sparks at different release sites in rat ventricular myocytes, J. Physiol. 505 (Pt 2) (1997) 337-344
- [41] K. Thurley, I.F. Smith, S.C. Tovey, C.W. Taylor, I. Paker, M. Falcke, Timescales of IP<sub>3</sub>-evoked Ca<sup>2+</sup> spikes emerge from Ca<sup>2+</sup> puffs only at the cellular level, Biophys. . 101 (11) (2011) 2638-2644.
- [42] E.A. Sobie, L.S. Song, W.J. Lederer, Local recovery of Ca<sup>2+</sup> release in rat ventricular myocytes, J. Physiol. 565 (2) (2005) 441-447.
- [43] D. Fraiman, S.P. Dawson, A model of the IP3 receptor with a luminal calcium binding site: stochastic simulations and analysis, Cell Calcium 35 (5) (2004) 403-
- [44] J. Sneyd, J.F. Dufour, A dynamic model of the type-2 inositol trisphosphate receptor, Proc. Natl. Acad. Sci. U.S.A. 99 (4) (2002) 2398-2403.
- G. Ullah, I. Parker, D.D. Mak, J.E. Pearson, Multi-scale data-driven modeling and observation of calcium puffs, Cell Calcium 52 (2) (2012) 152-
- [46] A.V. Zima, E. Picht, D.M. Bers, L.A. Blatter, Termination of cardiac Ca<sup>2+</sup> sparks: role of intra-SR [Ca<sup>2+</sup>], release flux, and intra-SR Ca<sup>2+</sup> diffusion, Circ. Res. 103 (8) (2008) e105-e115.
- [47] Y.X. Li, J. Rinzel, Equations for IP<sub>3</sub>R-mediated [Ca<sup>2+</sup>]<sub>i</sub> oscillations derived from a detailed kinetic model: a Hodgkin-Huxley like formalism, J. Theor. Biol. 166 (4) (1994) 461-473.
- [48] Y.D. Huang, S. Rüdiger, J.W. Shuai, Modified Langevin approach for a stochastic
- calcium puff model, Eur. Phys. J. B 83 (2011) 401–407. [49] S. Weinberg, G.D. Smith, The influence of Ca<sup>2+</sup> buffers on free [Ca<sup>2+</sup>] fluctuations and the effective volume of Ca<sup>2+</sup> microdomains, Biophys. J. 106 (12) (2014) 2693-